Long-time asymptotic states of forced two-dimensional barotropic incompressible flows on a rotating sphere

Obuse, Kiori; Takehiro, Shin-ichi; Yamada, Michio

PHYSICS OF FLUIDS **22**, 056601 (2010)

Long-time asymptotic states of forced two-dimensional barotropic incompressible flows on a rotating sphere

Kiori Obuse,[a] Shin-ichi Takehiro,[b] and Michio Yamada[c]
Research Institute for Mathematical Sciences, Kyoto University, Kyoto 606-8502, Japan

(Received 9 October 2009; accepted 11 March 2010; published online 12 May 2010)

This study re-examines a long-time asymptotic state of a two-dimensional barotropic incompressible flow with a small-scale, Markovian random forcing on a rotating sphere. Numerical simulations with different rotation rates of the sphere and different wavenumbers of the forcing are performed from zero initial condition. The integration time is extended to around 100–500 times that of the previous study by Nozawa and Yoden [Phys. Fluids **9**, 2081 (1997)]. At an early stage of the time integration, a multiple zonal-band structure or a structure with westward circumpolar jets emerges. However, in the course of time development, a multiple zonal-band structure is found to appear in all cases. The multiple zonal-band structure then enters quasisteady state, showing little energy increase with nearly steady energy spectrum. This is followed by a sudden merger/disappearance of the jets, accompanying an energy increase, and at the final stage of the time integration, a zonal-band structure with only two or three jets is realized in all cases. The characteristic total wavenumber of this asymptotic state is far lower than the Rhines wavenumber of the zonal flow, which suggests that the inverse energy cascade is not totally stopped by the β effect. © *2010 American Institute of Physics*. [doi:10.1063/1.3407652]

I. INTRODUCTION

Many studies on fluid dynamics in a nonrotating system have been performed in relation to fluid phenomena in an ordinary life. On the other hand, the fluid dynamics in a rotating system is also attracting much interest in respect, for instance, of observations in geoscience and of environmental problems. In these areas, there are plenty of mathematical models with a wide range of complexity in terms of the treatment of the physical processes. With the great progress in computer's performance these days, more and more realistic numerical simulations are performed by using such complex models. However, even the basic nature of simple mathematical models being the foundation of such complex models is not necessarily clear.

One of such unclear characteristics is a long-time asymptotic state of the system, which is one of the most interesting properties from the viewpoints of dynamics of planetary atmospheres and fluid dynamics. In this paper, we consider a long-time asymptotic state of a two-dimensional barotropic incompressible flow on a rotating sphere, which is one of the most fundamental dynamical models for planetary atmospheres.

It is well known that, when a system is not rotating, the energy is conserved in a three-dimensional system, whereas both the energy and the enstrophy are conserved in a two-dimensional system. As a consequence, in contrast to three-dimensional case, two-dimensional turbulence in a nonrotating system shows the enstrophy cascade and the inverse energy cascade, which brings about a larger-scale structure as time progresses.

By contrast, when the system has β effect, which is the consequence of the combination of the effect of the rotation and the spherical effect of the system, two-dimensional turbulence shows greatly different properties. Rhines[1] performed numerical experiments on a β plane and found that the multiple zonal-band structure, a structure with alternating westward and eastward jets, develops. Introducing the Rhines wavenumber at which the β effect and the advective effect in the governing equation become comparable, he explained the multiple zonal-band structure as a result of the arrest of the inverse energy cascade around the Rhines wavenumber.

Many succeeding studies have confirmed the emergence of the multiple zonal-band structure on both a β plane and a two-dimensional sphere.[2,3] The multiple zonal-band structure suggests many fascinating problems such as the mechanism of energy's concentration to zonal jets[4–6] and the asymmetry of the eastward and westward jets' profiles. However, it does not seem to be clear whether the long-time asymptotic state is actually characterized by such multiple zonal-band structure even in the cases on a β plane.

Recently, Yoden and Yamada[7] investigated the long-time asymptotic states of freely decaying two-dimensional barotropic incompressible flows on a rotating sphere. Interestingly, the long-time asymptotic states are not necessarily characterized by the multiple zonal-band structure but strong westward circumpolar jets become prominent after long-time integration, although there still exists weak multiple zonal-band structure in the low and middle latitudes. The scaling laws for this circumpolar jets are obtained by Takehiro *et al.*;[8] when the rotation rate of the sphere Ω increases, the

[a]Electronic mail: obuse@kurims.kyoto-u.ac.jp.
[b]Electronic mail: takepiro@gfd-dennou.org.
[c]Electronic mail: yamada@kurims.kyoto-u.ac.jp.

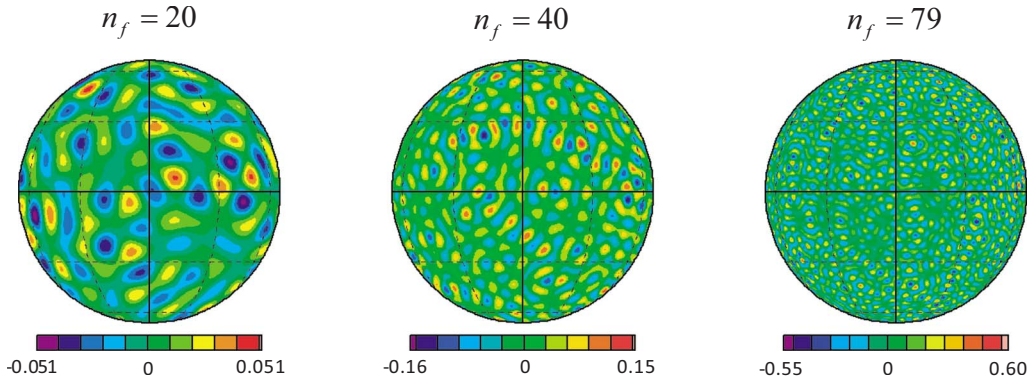

FIG. 1. (Color online) Vorticity forcing field at dimensionless time $t=1000$. n_f of the left, the middle and the right panels are 20, 40, and 79, respectively. The top of the sphere, the bottom of the sphere, and the center line correspond to the North Pole (90° N), the South Pole (90° S), and the equator, respectively.

strength of the jets increases as $\Omega^{1/4}$ and the width of the jets decreases as $\Omega^{-1/4}$.

On the other hand, for a forced two-dimensional barotropic incompressible flow on a two-dimensional sphere, Nozawa and Yoden[9] performed numerical simulations, with a Markovian random forcing, of 18 cases with different combinations of a rotation rate of the sphere and a forcing wavenumber. There, they showed that the generated flow fields are characterized by a multiple zonal-band structure or a structure with westward circumpolar jets. They also pointed out that the two different structures can arise according to the relative magnitude between the Rhines wavenumber of the flow and the forcing wavenumber, and also that when the forcing wavenumber is higher than the Rhines wavenumber, the inverse energy cascade continues until the characteristic wavenumber of the flow reaches around the Rhines wavenumber to form the multiple zonal-band structure; but when the forcing wavenumber is lower than the Rhines wavenumber, the inverse energy cascade hardly occurs, and the circumpolar jets appear as a result. In contrast, Huang *et al.*[10] performed simulations with a white noise forcing and obtained an asymptotic state consisting of only two zonal jets. They then inferred that the Markovian random forcing in Nozawa and Yoden[9] may be regarded as a strong drag with small wavenumber dissipation which maintains the formed multiple zonal-band structure.

The numerical time integration of Nozawa and Yoden,[9] however, does not seem to be long enough to obtain long-time asymptotic states since the observed jets appear to be still changing. Therefore, in this paper, we re-examine the long-time asymptotic states of the two-dimensional barotropic incompressible flows on a rotating sphere with a small-scale, homogeneous, isotropic, and Markovian random forcing. We extend the integration time of numerical simulation to about 100–500 times that of Nozawa and Yoden.[9] Section II shows the model used for the simulations, then the numerical results and the stability of some obtained asymptotic states are discussed in Sec. III, and the conclusion follows in Sec. IV.

II. EQUATION OF MOTION AND NUMERICAL METHOD

The model equation considered in this paper is a nondimensionalized vorticity equation for a forced two-dimensional barotropic incompressible flow on a rotating sphere, given in longitude ϕ and sine latitude μ,[11]

$$\frac{\partial \zeta}{\partial t} + J(\psi,\zeta) + 2\Omega\frac{\partial \psi}{\partial \phi} = F + \nu(\nabla^2 + 2)\zeta. \tag{1}$$

Here, t is time, ψ is the stream function, and $\zeta \equiv \nabla^2\psi$ is the vorticity, where ∇^2 is the horizontal Laplacian on a sphere. Ω is a dimensionless constant rotation rate of the sphere, ν is the dimensionless kinematic viscosity coefficient, and $F=F(\phi,\mu,t)$ is the vorticity forcing function. $J(A,B)$ is the Jacobian operator: $J(A,B) \equiv (\partial A/\partial\phi)(\partial B/\partial\mu) - (\partial A/\partial\mu) \times (\partial B/\partial\phi)$. The term $2\nu\zeta$ in the viscosity term is necessary for the conservation of total angular momentum of the system, as discussed in, for example, Bains.[12]

The vorticity forcing function F is taken to be the same as that in Nozawa and Yoden;[9] small-scale, homogeneous, isotropic, and Markovian random function is given by

$$F(\phi,\mu,j\Delta t) = RF[\phi,\mu,(j-1)\Delta t] + \sqrt{(1-R^2)}\hat{F}(\phi,\mu,j\Delta t), \tag{2}$$

where Δt is the time step interval, j is the number of the time step, and $R=0.982$ is the memory coefficient. $\hat{F}$ is a random vorticity source generated at each time step as

$$\hat{F}(\phi,\mu,j\Delta t) = \sum_{n=n_f-\Delta n}^{n_f+\Delta n} \sum_{\substack{m=-n \\ m\neq 0}}^{n} \hat{F}_n^m(j) Y_n^m(\phi,\mu), \tag{3}$$

where $\hat{F}_n^m$ is the expansion coefficient of $\hat{F}$ and Y_n^m is the spherical harmonic with total wavenumber n and zonal wavenumber m. The phase of $\hat{F}_n^m$ $(m \geq 0)$ is random and uniformly distributed on $[0,\ 2\pi]$. The amplitude of $\hat{F}_n^m$ $(m \geq 0)$ is also random with $\|F\| = \sqrt{\langle \hat{F}^2 \rangle}$ being a prescribed value, where $\langle \cdots \rangle$ denotes the spherical mean. Then $\hat{F}_n^{-m}$ $(m>0)$ is the complex conjugate of $\hat{F}_n^m$ $(m>0)$ since $\hat{F}$ is

TABLE I. Ω, n_f, $\|F\|$, and integration time in each run. Run numbers correspond to those in Nozawa and Yoden (Ref. 9).

Run No.	Ω	n_f	$\|F\|$	Integration time
2	0.5π			1×10^5
3	π			1×10^5
4	2π	20	1.412×10^{-2}	1×10^5
5	4π			1×10^5
6	8π			1×10^5
8	0.5π			1×10^5
9	π			1×10^5
10	2π	40	3.929×10^{-2}	1.2×10^5
11	4π			2.5×10^5
12	8π			1.6×10^5
14	0.5π			1×10^5
15	π			1×10^5
16	2π	79	1.415×10^{-1}	5.3×10^5
17	4π			5.2×10^5
18	8π			5.7×10^5

real. This vorticity forcing is given in a narrow band in the wavenumber space: $n_f-\Delta n\le n\le n_f+\Delta n$ with $\Delta n=2$. Figure 1 shows the examples of the vorticity forcing fields with $n_f=20$, 40, and 79, and $\Delta t=0.05$.

For numerical calculations, the parameters in the governing equation (1) are all set equal to those used in Nozawa and Yoden.[9] The kinematic viscosity coefficient is $\nu=3.46\times10^{-6}$. The rotation rate of the sphere Ω takes five different values; $\Omega/\Omega_J=0.25$, 0.5, 1.0, 2.0, and 4.0, with $\Omega_J\equiv2\pi$. The central total wavenumber of the forcing n_f takes three different values $n_f=20$, 40, and 79, and for each of n_f, the rms amplitude of $\hat{F}$, i.e., $\|F\|$ is given, as shown in Table I.[13]

A spectral method with the spherical harmonics is used for the calculation. The stream function ψ is expanded as

$$\psi(\phi,\mu,t)=\sum_{n=0}^{N_T}\sum_{m=-n}^{n}\psi_n^m(t)Y_n^m(\phi,\mu)$$
$$=\sum_{n=0}^{N_T}\sum_{m=-n}^{n}\psi_n^m(t)P_n^m(\mu)\exp(im\phi).$$

Here, ψ_n^m is the expansion coefficient. We set the truncation wavenumber to be $N_T=199$, then we take 600 and 300 spatial grid points in the longitudinal and latitudinal directions, which are sufficiently large to eliminate the aliasing errors. Linear terms in the governing equation are analytically treated by using exponential function. The time integration is performed with the fourth order Runge–Kutta method with a time step interval $\Delta t=0.05$ from the initial condition $\zeta=0$. The integration time is extended to about 100–500 times that of Nozawa and Yoden[9](Table I). With the conditions above, 15 simulations with different combinations of Ω and n_f (Table I) are performed.[14] Note that the run numbers are 2–6, 8–12, and 14–18, which keep the numbering correspondence between the simulations of Nozawa and Yoden[9] and ours.

III. RESULTS OF NUMERICAL EXPERIMENTS

A. Zonal-mean zonal angular momentum

We first observe temporal development of zonal-mean zonal angular momentum $\overline{[L_{\rm lon}]}$ in $0\le t\le1000$. Here, $\overline{[\cdots]}$ denotes the zonal mean and $\overline{[L_{\rm lon}]}$ is given by

$$\overline{[L_{\rm lon}]}\equiv\frac{1}{2\pi}\int_0^{2\pi}u_{\rm lon}\sqrt{1-\mu^2}d\phi,$$

where $u_{\rm lon}=-\sqrt{1-\mu^2}(\partial\psi/\partial\mu)$ is the longitudinal component of velocity.

Figure 2 corresponds to the main result of Nozawa and Yoden,[9] who discussed the flow pattern by using the numerical integration from $t=0$ to 1000. On runs 2, 3, 8–11, and 14–18, a structure with alternating eastward and westward zonal jets, which we call a multiple zonal-band structure, is formed, while westward circumpolar jets and the weak eastward flow at low—midlatitude appears on runs 4–6, and 12. These results are in agreement with those of Nozawa and Yoden.[9]

Then we continue the time integrations further to $t=1.0\times10^5$ or more, which is at least 100 times as long as the integration time of Nozawa and Yoden.[9] Figure 3 shows the temporal development of zonal-mean zonal angular momentum $\overline{[L_{\rm lon}]}$. It is apparent that, in all cases, in spite of the classification made at $t=1000$ by Nozawa and Yoden,[9] a multiple zonal-band structure appears in the course of time development and then enters a quasisteady state with little change in its flow pattern, followed by a sudden merger/disappearance of the jets. In most cases, two prograde jets merge and a retrograde jet between the two prograde jets disappears. At the final stage of the time integration, a zonal-band structure with only a few broad zonal jets is realized; two jets remain in runs 2–6, 8–12, 14, and 15, and three jets in runs 16–18. The structure with two broad jets, which consists of an eastward and a westward jets, shows no correlation with whether the eastward jet covers the Northern hemisphere or the Southern hemisphere.

There is a tendency that the integration time needed to reach the structure with a few zonal jets becomes longer as the forcing wavenumber n_f becomes higher and the rotation rate Ω becomes larger. For example, when $n_f=20$, the case with $\Omega=4\pi$ (run 5) and the case with $\Omega=8\pi$ (run 6) require 4×10^4 and 8×10^4 dimensionless time to get to the structure with two broad jets, respectively. Also, for instance, when $\Omega=4\pi$, the case with $n_f=20$ (run 5), 40 (run 11) require 4×10^4 and 2×10^5 dimensionless time to form the structures with two broad jets, and the case $n_f=79$ (run 17) takes 3×10^5 dimensionless time even to get to the structure with three broad jets.

It is interesting to note that, in most of the cases, eastward jets merge, while a westward jet disappears. In the process of the merger/disappearance of the jets, only one of the two merging jets becomes very strong and intrudes into the other, intercepting the development of the middle jet.

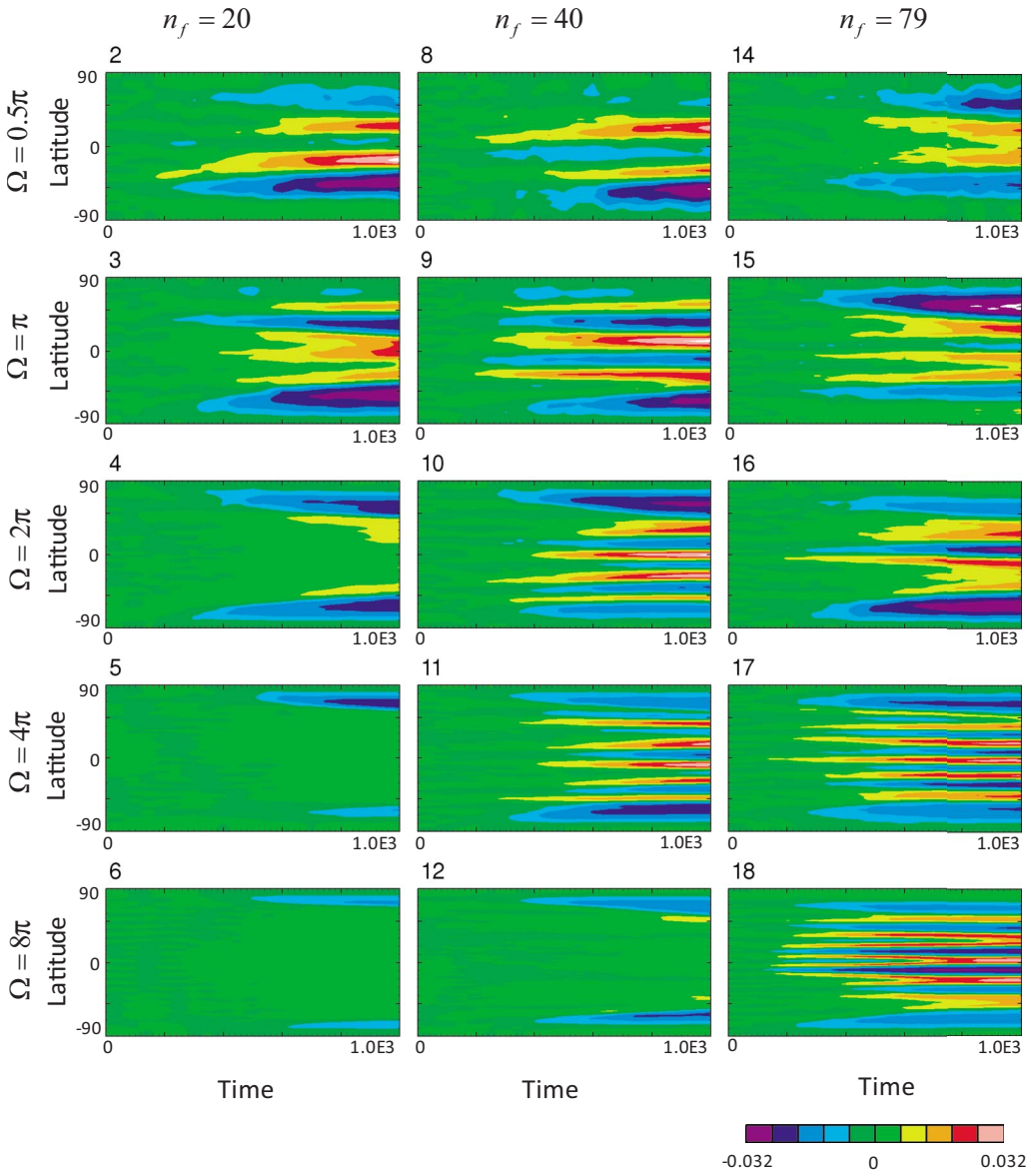

FIG. 2. (Color online) Temporal development (t=0–1000) of zonal-mean zonal angular momentum $\overline{[L_{\rm lon}]}$. The horizontal and the vertical axes in each panel are, respectively, time and latitude in linear scale. This corresponds to Fig. 3 in Nozawa and Yoden (Ref. 9).

It is widely known that when the state is still with a multiple zonal-band structure, there exist significant asymmetries between eastward and westward jets in terms of their strength and width. Nevertheless, at sufficiently large time, there are no apparent asymmetries between the two (or three) broad jets.

The structure with two broad zonal jets is one of the long-time asymptotic states of the system. The inverse cascade does not proceed any more, and the two zonal jets cannot merge to one zonal jet because of the conservation law of the total angular momentum of the system. Therefore, according to our numerical results, the asymptotic states of the flow in runs 2–6, 8–12, 14, and 15 consist of two broad zonal jets dominating over the whole sphere. On the other hand, the final states in runs 16, 17, and 18 consist of three broad zonal jets, but it is not clear whether or not the three jets further merge or disappear at a later time. This will be discussed again in Sec. III F.

B. Energy of zonal flow

The details of the appearance of the structure with a few zonal jets are observed in the temporal variation in the spectral distribution of the energy of zonal flow

$$\langle \mathcal{E}_z(n,t) \rangle \equiv \tfrac{1}{2} n(n+1) |\psi_n^0(t)|^2.$$

For instance, from the temporal development of $\langle \mathcal{E}_z \rangle$ in run 2 (not shown), it is confirmed that at an early stage of the time integration ($t \sim 100$), wavenumbers around the forcing wavenumber (n_f=20) possess the zonal energy. The energy-containing wavenumbers then decrease, and at $t \sim 500$, the total wavenumbers n=3 and 7 mainly possess the zonal energy. At $t \sim 1000$, the zonal energy at n=3 is the strongest, and this state remains stable until $t \sim 2.4 \times 10^4$, when most of the zonal energy speedily cascade to n=2. Then the temporal

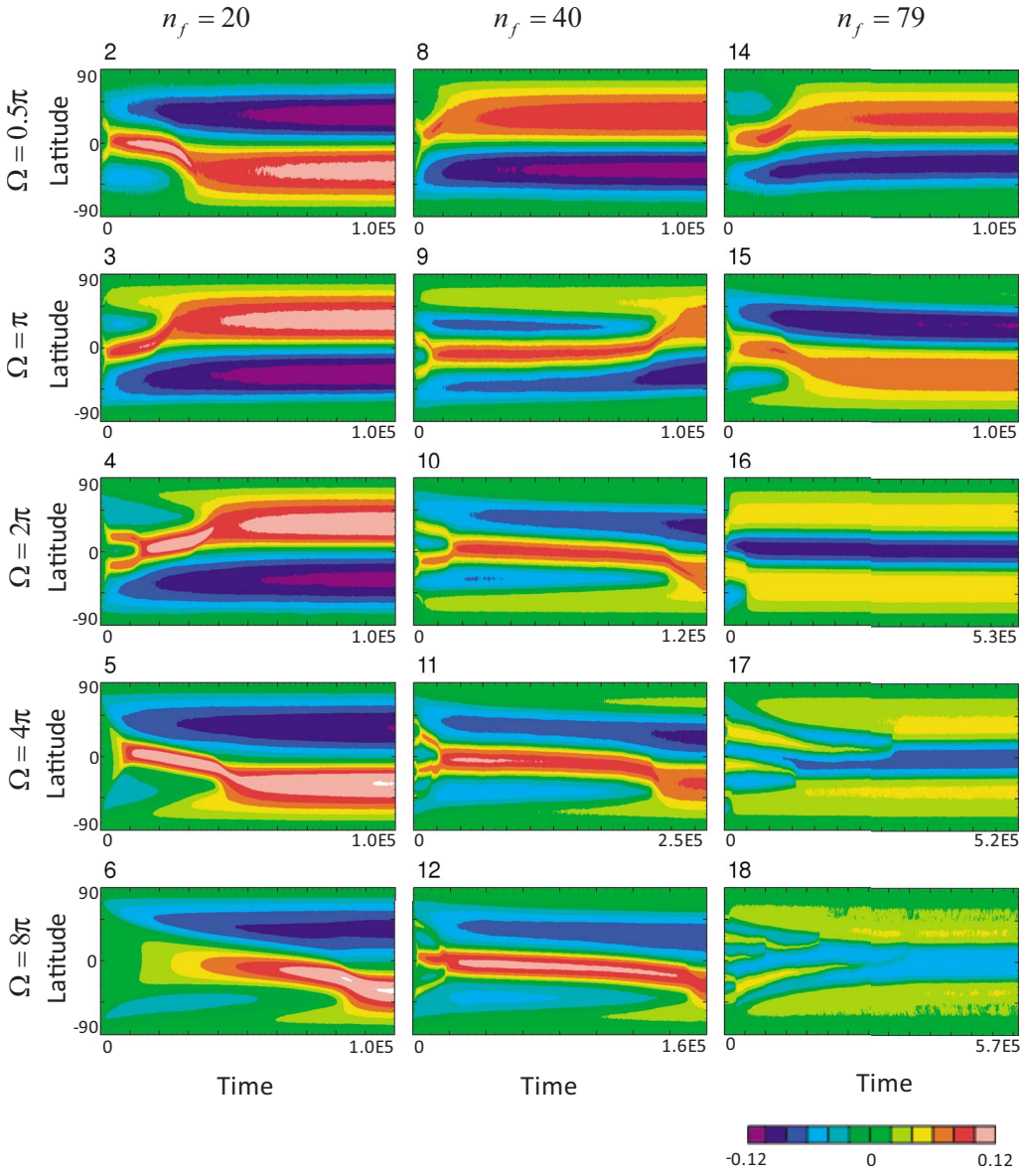

FIG. 3. (Color online) Long-time development of the zonal-mean zonal angular momentum $\overline{[L_{\mathrm{lon}}]}$. The horizontal and the vertical axes in each panel are, respectively, time and latitude in linear scale. The temporal integrations have performed $t=0-1\times10^5$ in runs 2–6, 8, 9, 14, and 15, $t=0-1.2\times10^5$ in run 10, $t=0-2.5\times10^5$ in run 11, $t=0-1.6\times10^5$ in run 12, $t=0-5.3\times10^5$ in run 16, $t=0-5.2\times10^5$ in run 17, and $t=0-5.7\times10^5$ in run 18.

variations in $\langle\mathcal{E}_z\rangle$ from $t=0$ to the final integral times in all runs (not shown) show that although energy-containing wavenumbers experience a long quasisteady period at $n\geq3$, they resume transferring their energy to lower wavenumbers and eventually reach 2 (runs 2–6, 8–12, 14, and 15) or 3 (runs 16–18).

C. The Rhines wavenumber

In Nozawa and Yoden,[9] the main total wavenumbers n of the energy of the zonal flow $\langle\mathcal{E}_z\rangle$ spread over a quite wide range $2\lesssim n\lesssim n_\beta$ at $t=1000$, where n_β is the Rhines wavenumber. Since, in all runs, the inverse energy cascades proceed further than those in Nozawa and Yoden,[9] we examine the temporal change in the Rhines wavenumber n_β on a sphere, which is defined by

$$n_\beta(t) \equiv \sqrt{\frac{\langle\beta\rangle}{2U_{\mathrm{rms}}(t)}}. \tag{4}$$

Here, $U_{\mathrm{rms}}(t)$ is the rms velocity of the fluid,

$$U_{\mathrm{rms}}(t) \equiv \sqrt{2\mathcal{E}(t)},$$

and $\langle\beta\rangle=\pi\Omega/2$ denotes the spherical mean of β, the latitudinal gradient of the Coriolis parameter. Also, we define the energy-weighted mean total wavenumber n_{mean} as the characteristic total wavenumber of the flow,

$$n_{\mathrm{mean}}(n,t) \equiv \frac{\Sigma_{n=1}^{N_T} n\langle\mathcal{E}_{\mathrm{tot}}(n,t)\rangle}{\Sigma_{n=1}^{N_T}\langle\mathcal{E}_{\mathrm{tot}}(n,t)\rangle},$$

where $\langle\mathcal{E}_{\mathrm{tot}}\rangle$ is given by

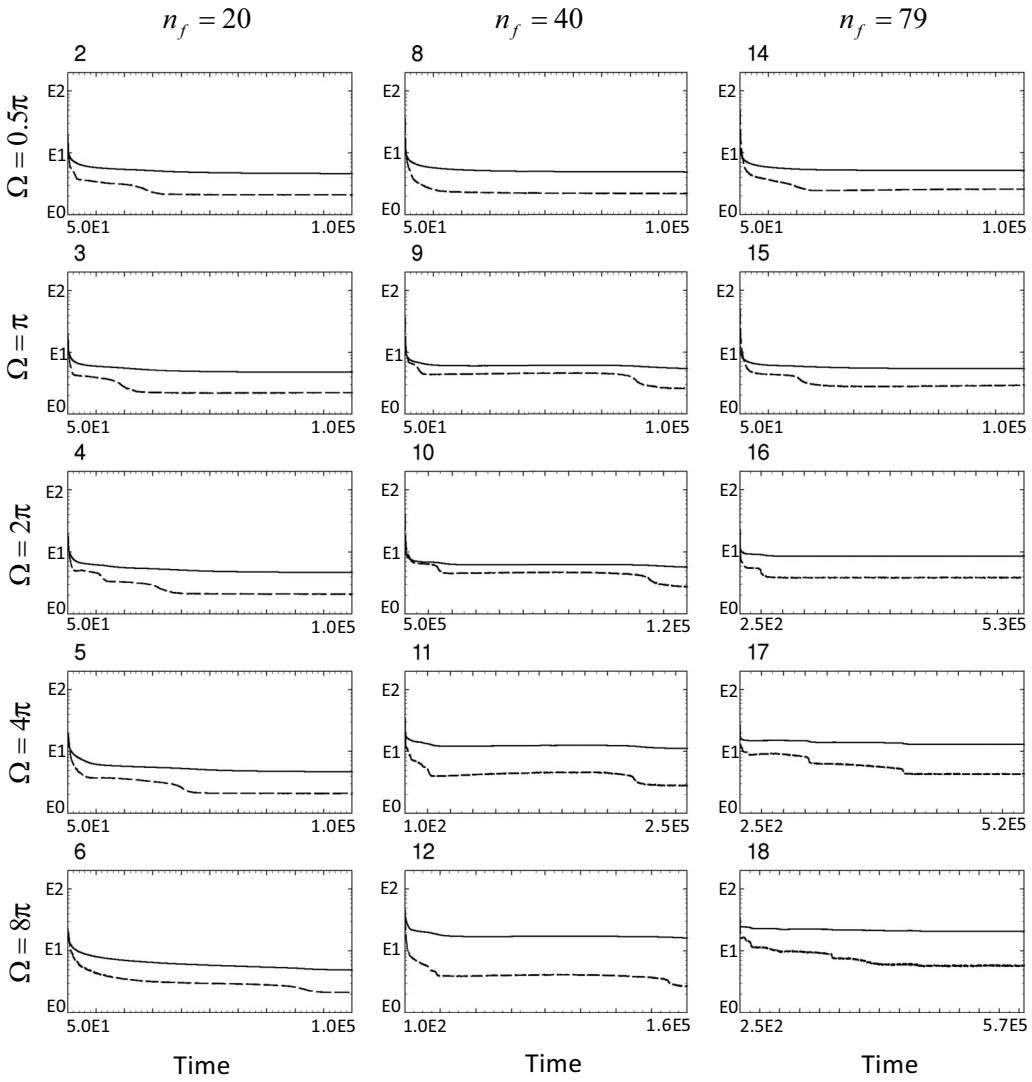

FIG. 4. Temporal variation in the Rhines wavenumber n_β (solid line) and the characteristic wavenumber n_{mean} (dashed line). The horizontal and the vertical axes in each panel are time in linear scale and the Rhines wavenumber and the characteristic wavenumber in log scale, respectively. Note that n_β is infinity at $t=0$ because $\mathcal{E}(0)=0$. The temporal integrations have performed $t=0-1\times10^5$ in runs 2–6, 8, 9, 14, and 15, $t=0-1.2\times10^5$ in run 10, $t=0-2.5\times10^5$ in run 11, $t=0-1.6\times10^5$ in run 12, $t=0-5.3\times10^5$ in run 16, $t=0-5.2\times10^5$ in run 17, and $t=0-5.7\times10^5$ in run 18.

$$\langle \mathcal{E}_{\mathrm{tot}}(n,t)\rangle \equiv \frac{1}{2}\sum_{m=-n}^{n} n(n+1)|\psi_n^m(t)|^2,$$

which means the energy at the total wavenumber n.

The temporal variation in n_β and n_{mean} is shown in Fig. 4. The characteristic wavenumber n_{mean} becomes lower than the Rhines wavenumber n_β in a very early stage of the time integration (before $t=1000$) and decreases to reach finally a fairly low wavenumber (2–6) at the final stage. Note that n_{mean} does not reach 2 precisely even when the fully developed two broad jets are dominating over the sphere.

The above results suggest that the inverse energy cascade or the energy transfer to lower wavenumbers continues even when $n_{\mathrm{mean}}<n_\beta$, for the flow field finally to consist of only a few (two or three) broad zonal jets. This also suggests that the Rhines wavenumber does not give an estimation of the characteristic wavenumber of the asymptotic flow field.

D. The total energy

Figure 5 shows the temporal variation in the spherical-mean energy,

$$\langle \mathcal{E}(t)\rangle \equiv \frac{1}{4\pi}\int_0^{2\pi}\int_{-1}^{1}\frac{u_{\mathrm{lon}}^2+u_{\mathrm{lat}}^2}{2}d\mu d\phi = \frac{1}{2}\sum_{n=0}^{N_T}\sum_{m=-n}^{n} n(n+1)|\psi_n^m(t)|^2, \quad (5)$$

where N_T is the truncation wavenumber. The most impressive feature is the stepwise increase of $\langle\mathcal{E}\rangle$ seen in runs 9–12 and 15–18. As Huang *et al.*[10] pointed out, $\langle\mathcal{E}\rangle$ experiences quasisteady states with no apparent energy increase in these runs. However, the quasisteady state is followed by a sudden increase in energy (except the last stairs in runs 16–18). This implies that the standstill of the energy increase is not an

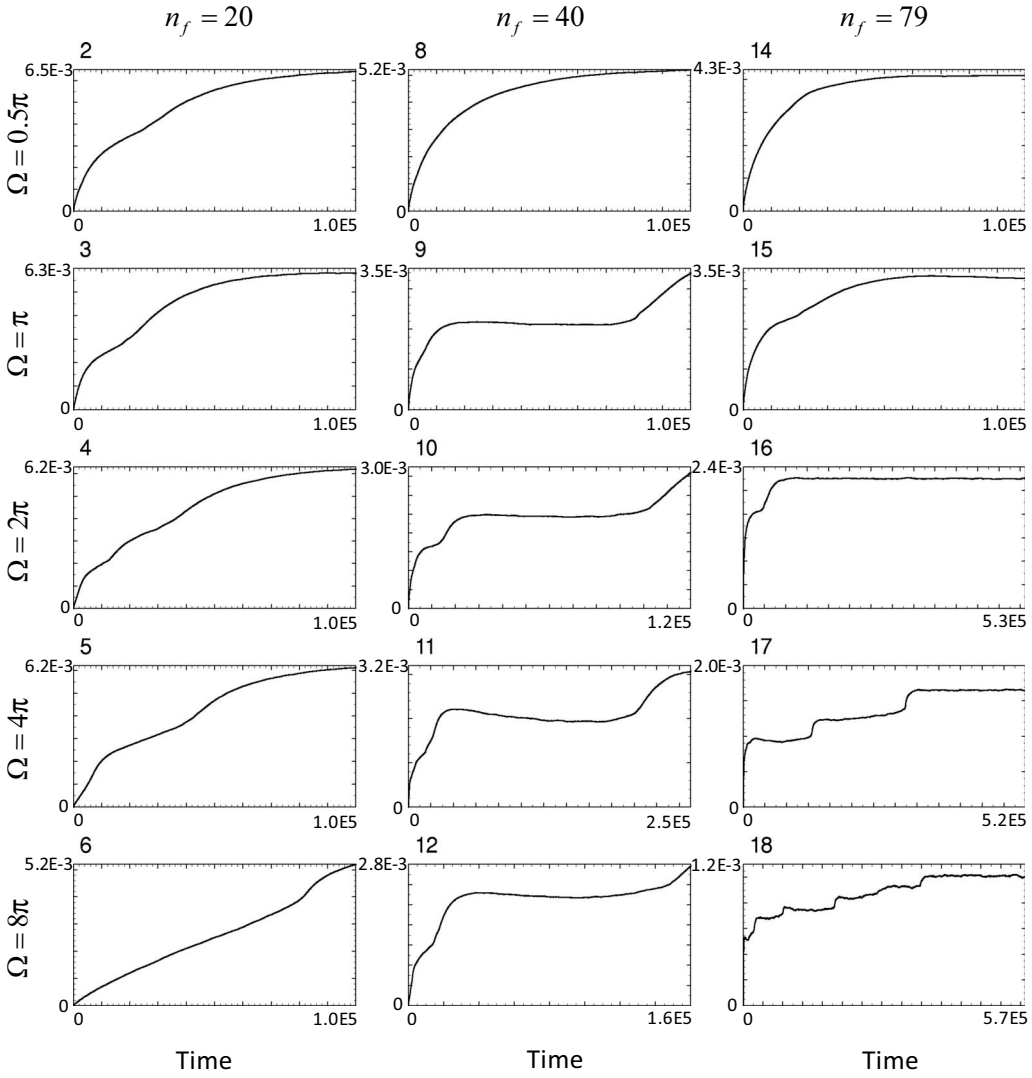

FIG. 5. Temporal variation in spherical-mean energy $\langle \mathcal{E} \rangle$. The horizontal and the vertical axes in each panel are, respectively, time and energy in linear scale. The temporal integrations have performed $t=0-1\times10^5$ in runs 2–6, 8, 9, 14, and 15, $t=0-1.2\times10^5$ in run 10, $t=0-2.5\times10^5$ in run 11, $t=0-1.6\times10^5$ in run 12, $t=0-5.3\times10^5$ in run 16, $t=0-5.2\times10^5$ in run 17, and $t=0-5.7\times10^5$ in run 18.

effective sign of the realization of an asymptotic state. It is interesting that the temporal variation in energy and the temporal development of jets have almost perfect correspondence in two aspects; the period in which the energy shows little increase coincides with the period in which the number of the jets remains constant; the time when the energy suddenly restarts increasing coincides with the time when the jets suddenly merge/disappear.[15] On the other hand, in runs 2–6, 8, and 14, where the zonal-mean zonal angular momentum $\overline{[L_{\mathrm{lon}}]}$ shows a gradual formation of two broad jets in Fig. 3, $\langle \mathcal{E} \rangle$ also increase gradually, and the stepwise behavior is not observed. These results imply that the merger/disappearance of jets bring about the energy increase.

Concerning the asymptotic states of the flow, in the run where two broad jets are finally formed (runs 2–6, 8–12, 14, and 15), we can see a tendency that after the two broad jets are formed, $\langle \mathcal{E} \rangle$ keeps increasing for a while and then slowly relaxes it. This implies that it is still not obvious whether the 3-jet state at its final integral time in runs 16–18 is the asymptotic state, or still a transient state before the next merger/disappearance.

E. Stream function

Lastly, we observe the stream function and the zonal velocity on the sphere. In all runs, the zonal flow structure becomes dominant from an early stage of time development. At around the time of the appearance of the zonal-band structure in Fig. 3, the structure with alternating rather eastward and westward flows are also formed on a sphere (not shown). As time goes on, these flows become more zonal undergoing mergers/disappearances, and fairly zonal flows have formed by the final integration times in most runs (not shown), although some large-scale and nonzonal equatorial flows, which are spoiling the zonal flows, are seen (runs 2, 8, and 14), and there are several small nonzonal flows in the regions between the eastward and the westward flows (runs 15 and

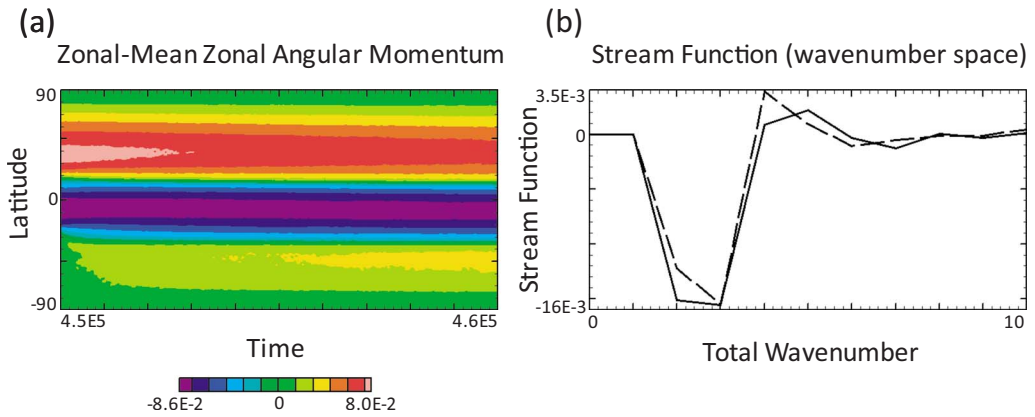

FIG. 6. (Color online) (a) Temporal developments of $[\overline{L_{\rm lon}}]$. The horizontal and the vertical axes are, respectively, time and latitude in linear scale. (b) ψ_n^0 $(0 \le n \le 10)$ at $t=4.5\times10^5$ (solid line) and $t=4.6\times10^5$ (dashed line). The horizontal and the vertical axes are, respectively, total wavenumber and the stream function in linear scale. The flow is set to have ψ_2^0 ten times as large as that in run 17 at $t=4.5\times10^5$.

16). The early emergence of the zonal-band structure through the mergers/disappearances of the jets may tempt us to interpret it as a consequence of a barotropic instability of the jet. However, it should be remarked that, as pointed out by Rhines,[1] a laminar zonal jet with a meridional scale larger than the Rhines scale is linearly stable owing to Rayleigh's condition. Therefore, nonzonal flows superimposed on the zonal jets appear necessary for the merger/disappearance of the jets.

F. Stability of the 3-jet structure

As we have seen in Sec. III A, the structures with three zonal jets seen in runs 16–18 are persistent and show little change for nearly 3×10^5 of time, whereas the asymptotic states consist of two broad jets in the rest of the runs. It is not clear if the broad 3-jet state is the asymptotic state of the system. Here, we examine the robustness of the 3-jet state in run 17 by adding small perturbation with $(n,m)=(2,0)$ to the stream function, since the main component of the stream function of the 2-jet state in the wavenumber space is the one with $n=2$, and observe whether the three jets experience a merger/disappearance to two jets or not. The solid line in Fig. 6(b) shows the stream function at $t=4.5\times10^5$ in run 17. Now let us magnify the $(n,m)=(2,0)$ component of this stream function two, three, five, and ten times, then make temporal development taking each of the flows as the starting flow field at $t=4.5\times10^5$. The obtained results show that, in all cases, the three jets do not experience merger/disappearance and are persistent until the final time [for the case with ψ_2^0 ten times as large as that in run 17 at $t=4.5\times10^5$ is shown in Fig. 6(a)]. On the contrary, $[\overline{L_{\rm lon}}]$ appears to go back to the 3-jet state even when the starting flow field consists of two strong jets and a very weak jet, the third (the weakest) jet is enhanced in the course of temporal development, and the 3-jet state is reproduced at $t=4.6\times10^5$. In fact, as shown in Fig. 6(b), the absolute value of the $(n,m)=(2,0)$ component of the stream function decreases, and the $(n,m)=(4,0)$ component increases instead.

IV. DISCUSSIONS AND CONCLUSIONS

In Secs. II and III, we have performed 15 numerical simulations with the Markovian random forcing, with different combinations of the rotation rate of a sphere Ω and the central total wavenumber of the forcing n_f. We have integrated the equation of motion numerically from $t=0$ to $t=1.0\times10^5$ (100 times of the integration time of Nozawa and Yoden[9]) or even more, with the zero initial condition. At an early stage of the integration, in line with the findings of Nozawa and Yoden,[9] a multiple zonal-band structure or a structure with westward circumpolar jets emerges. However, in the course of further time development, a multiple zonal-band structure appears in all runs and then enters a quasi-steady state, showing little energy increase with nearly steady spectral distribution of the energy, followed by a sudden merger/disappearance of the jets, accompanying an energy increase. At the final stage of the time integration, a zonal-band structure with only a few (two or three) zonal jets were realized in each case. This affects the spectral distribution of the zonal energy, which shows the strong energy concentration to the total wavenumber $n=2$ or 3 (this n coincides with the number of the jets) at the final integration time. At the final stage, the characteristic total wavenumber is lower than the Rhines wavenumber of the flow.

The numerical results show that the 2-jet state obtained here is one of the long-time asymptotic states of the two-dimensional barotropic incompressible flow with a small-scale, homogeneous, isotropic, and Markovian random forcing on a rotating sphere, as the energy inverse cascade cannot reach the wavenumber $n=1$ due to the conservation law of the total angular momentum. Contrary to this, it is not clear whether the 3-jet state at the final integration time is the asymptotic state or it is still changing to the 2-jet state. In Sec. III F, we considered the stability of the 3-jet state to the perturbation with wavenumber $(n,m)=(2,0)$, and the result suggests that the 3-jet state may be possible to be one of the asymptotic states.

Huang *et al.*[10] argued that the inverse energy cascade reaches below the Rhines wavenumber when the forcing is

white noise, but not definitely when it is a Markovian random forcing. In our case of Markovian random forcing, the inverse energy cascade does not stop around the Rhines wavenumber but proceeds down to lower wavenumbers in the course of long-time evolution. This, together with the numerical result of Huang *et al.*,[10] suggests that, in the forced two-dimensional barotropic incompressible flow on a rotating sphere, the inverse energy cascade cannot be arrested around the Rhines wavenumber by the β effect irrespective of the kind of the forcing given to the system, and the asymptotic state consists of a very small number of zonal jets. This may also imply that a forced two-dimensional barotropic incompressible flow on a rotating sphere is not an appropriate model for the dynamics of the planetary atmospheres with multiple zonal-band structure such as the one seen on the Jupiter, as far as long-time asymptotic states are concerned.

Last but not least, although the real flow on a sphere becomes zonal to some degree even at an early stage of the time integration, the mergers/disappearances of the zonal jets seen in the simulations in this paper are not explained by the barotropic instability, as the laminar zonal jets have a meridional scale larger than the Rhines scale, and are therefore linearly stable as discussed in Sec. III F. This strongly suggests that the turbulence behind the zonal jets is essential for the mergers/disappearances of the zonal jets, although the energy is almost concentrated in the zonal components.

ACKNOWLEDGMENTS

The main part of the numerical model used in this study was constructed with a spectral transformation library "ISPACK" (http://www.gfd-dennou.org/library/ispack/) and a FORTRAN90 wrapper library "SPMODEL" (http://www.gfd-dennou.org/library/spmodel/). "gt4f90io" (http://www.gfd-dennou.org/library/gtool4/) and "NetCDF" (http://www.unidata.ucar.edu/packages/netcdf/) libraries were used for data IO routine of the model. The data analyses and the visualizations in this paper were done with the software products of the GFD Dennou Ruby project (http://ruby.gfd-dennou.org/). The numerical calculation was performed by the computer systems of the Research Institute for Mathematical Sciences, Kyoto University.

We would like to thank Dr. T. Nozawa for having shown his simulation code.

[1] P. B. Rhines, "Waves and turbulence on a beta-plane," J. Fluid Mech. **69**, 417 (1975).
[2] G. K. Vallis and M. E. Maltrud, "Generation of mean flows and jets on a beta plane and over topography," J. Phys. Oceanogr. **23**, 1346 (1993).
[3] G. P. Williams, "Planetary circulations: 1. Barotropic representation of Jovian and terrestrial turbulence," J. Atmos. Sci. **35**, 1399 (1978).
[4] A. Chekhlov, S. A. Orszag, S. Sukoriansky, B. Galperin, and I. Staroselsky, "The effect of small-scale forcing on large-scale structures in two-dimensional flows," Physica D **98**, 321 (1996).
[5] H.-P. Huang and W. A. Robinson, "Two-dimensional turbulence and persistent zonal jets in a global barotropic model," J. Atmos. Sci. **55**, 611 (1998).
[6] A. M. Balk, "Angular distribution of Rossby wave energy," Phys. Lett. A **345**, 154 (2005).
[7] S. Yoden and M. Yamada, "A numerical experiment on two-dimensional decaying turbulence on a rotating sphere," J. Atmos. Sci. **50**, 631 (1993).
[8] S. Takehiro, M. Yamada, and Y. Hayashi, "Energy accumulation in easterly circumpolar jets generated by two-dimensional barotropic decaying turbulence on a rapidly rotating sphere," J. Atmos. Sci. **64**, 4084 (2007).
[9] T. Nozawa and S. Yoden, "Formation of zonal band structure in forced two-dimensional turbulence on a rotating sphere," Phys. Fluids **9**, 2081 (1997).
[10] H.-P. Huang, B. Galperin, and S. Sukoriansky, "Anisotropic spectra in two-dimensional turbulence on the surface of a rotating sphere," Phys. Fluids **13**, 225 (2001).
[11] In the case of Jovian atmosphere, Eq. (1) has been obtained $a_J=7.00\times10^7$ m as length scale, and one Jovian day, 1 Jday$=3.57\times10^4$ s, as time scale, and thus the nondimensional rotation rate is $\Omega_J=2\pi$.
[12] I. Silberman, "Planetary waves in the atmosphere," J. Meteorol. **11**, 27 (1954).
[13] As Nozawa and Yoden (Ref. 9) used different normalizing coefficients of the spherical harmonics for vorticity forcing from those for other variables, $\|F\|$ has to correspond to the value $\sqrt{2}$ times larger than those used by Nozawa and Yoden (Ref. 9) in our calculation using the same normalizing coefficients for all variables. We greatly thank Dr. Nozawa for having kindly shown us his simulation code.
[14] The convergence of the numerical simulations in this paper has been checked by performing calculations with different parameters; $\Delta t=0.025$, which is half of the one used here; the trancation wavenumber is $N_T=341$ and number of the spatial grid points are 1024×512 which realize almost twice higher resolution than the one here.
[15] We note that this correspondence is also found in the temporal variation in the characteristic wavenumber n_{mean} in Fig. 4.